17th World Conference on Earthquake Engineering, 17WCEE
Sendai, Japan - September 13th to 18th 2020

A TENTATIVE PROCEDURE TO ASSESS THE SEISMIC RESIDUAL CAPACITY OF REINFORCED CONCRETE BUILDINGS

A. Cuevas[1], S. Pampanin[2]

[1] *Associate, Thornton Tomasetti Inc., acuevas@thorntontomasetti.com*
[2] *Professor, La Sapienza University of Rome, stefano.pampanin@uniroma1.it*

Abstract

This paper provides a description of the various factors affecting the residual fatigue life at a component (i.e., plastic hinge) level. It also presents a tentative formulation based on a numerical finite element investigation that relates the maximum and residual crack widths, and steel strain at peak displacement once the onset of nonlinearity has been exceeded. Preliminary equations to quantify the various factors are proposed.

Keywords: crack width, low-cycle fatigue, strain ageing, reinforced concrete plastic hinges, residual capacity

1. Introduction

According to capacity design principles developed in the 1960s, structures are designed to withstand major earthquakes by developing inelastic action and energy dissipation in concentrated regions known as plastic hinges. This in turn and consistent with the current design practice, leads to structural damage, often irreparable following a design earthquake level. Despite the availability of seismic assessment and rehabilitation guidelines, they are mainly focused on the evaluation of pre-damaged existing buildings. Very little information is available for assessing the residual capacity of relatively modern damaged buildings, even when they are designed following capacity design principles. When available, they provide an incomplete assessment from a fatigue life standpoint. The latter is particularly important for assessing the ability of a standing building to resist aftershocks once a big portion of their initial capacity has been consumed during the mainshock, and thus support the complex decision-making process of how and whether or not to make safe (i.e., repair and/or retrofit) or demolish.

One of the most controversial issues highlighted by the 2010-2011 Canterbury earthquakes sequence is the complexity and lack of knowledge and guidelines for an adequate evaluation of the reduced capacity of a damaged building compared to its pre-earthquake condition. As a more important corollary, the absolute term of the post-earthquake (or residual capacity) is of critical importance to: a) determine the new vulnerability of the building; and b) evaluate its capacity to sustain subsequent aftershocks and/or other design level event during the remaining life-time of the building. Arguably, partly but not exclusively as a result of such lack of knowledge and guidelines on the evaluation of the residual capacity and on the selection of appropriate repairing techniques, many modern buildings, in a number somehow exceeding common expectation, have ended up being demolished.

2. Factors affecting the residual fatigue life at a component level

This Section provides a description of the various factors affecting the residual fatigue life at a component (i.e., plastic hinge) level. Although these concepts can be extended to a more general situation, it has been specifically developed for well-detailed beams failing in flexure with a stable hysteretic behaviour. These factors are conceptually expressed in terms of coefficients and sketched in figures, and where applicable, equations to quantify them are also included. Figure 1 shows a typical reinforced concrete beam cross-section and its moment-curvature relationships obtained through section analysis, a comparison between the

original and damaged moment-curvature relationships, a comparison between unaged and aged steel stress-strain curves, and conceptual factors to account for stiffness deterioration, reduction in ductility, the increase in strength due to ageing, as well as cyclic and bond deterioration.

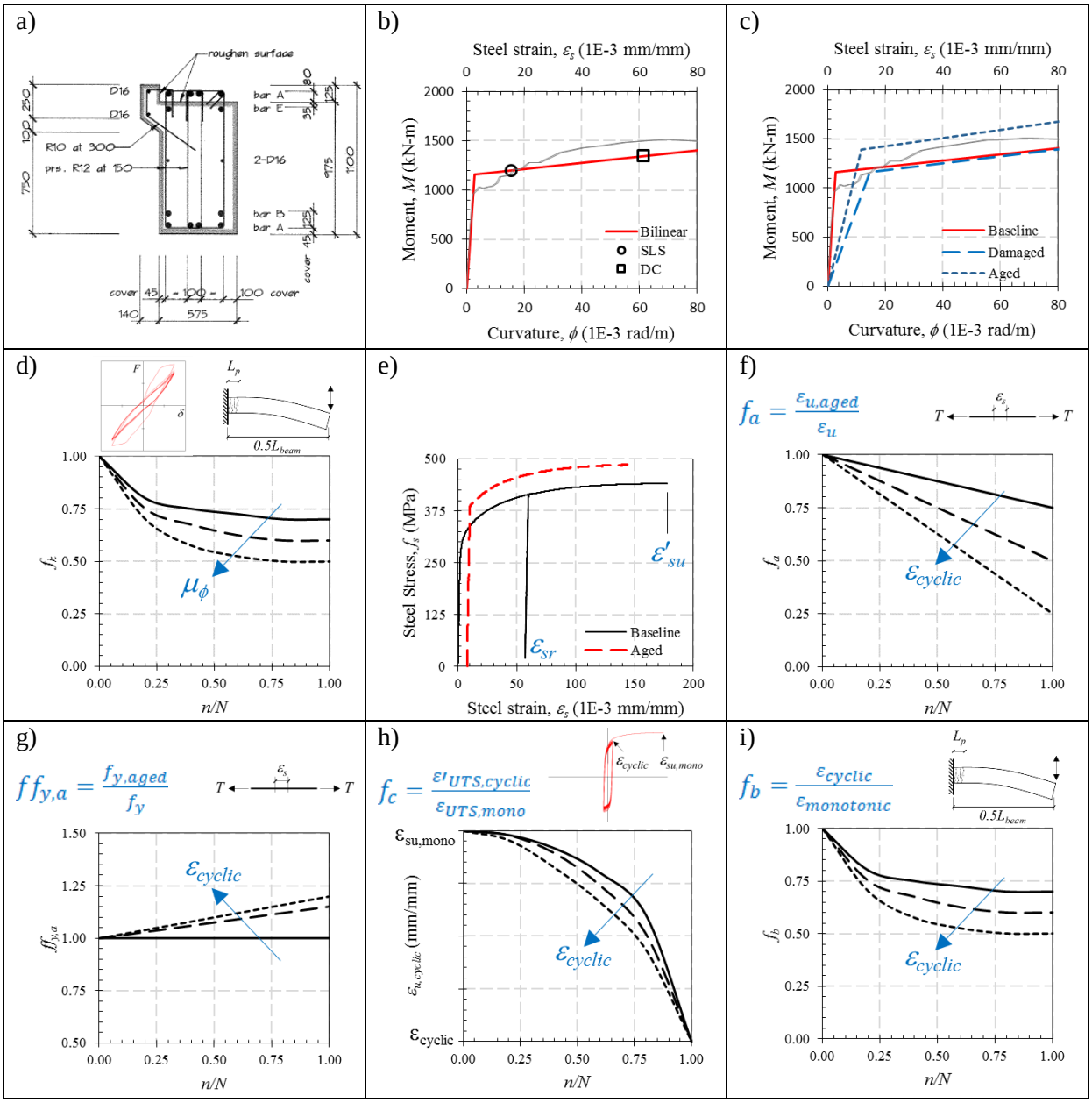

Figure 1 – a) Reinforced concrete beam cross-section; b) its moment-curvature; c) comparison between original and damaged moment-curvatures; d) conceptual factor to account for stiffness deterioration; e) comparison between unaged and aged steel stress-strain curves; f) conceptual factors to account for reduction in ductility; g) increase in strength due to ageing; h) cyclic deterioration; and i) bond deterioration.

2.1. Fatigue life

As stated in [12], fracture of longitudinal reinforcement due to low-cycle fatigue might be one of the most typical failure modes that can occur in flexural members during an earthquake, especially for structures located in mid-to-high seismic zones when one-to-five fully reversed cycles of large strain equi-amplitudes up to ε_s= 0.06 mm/mm or 6% may be expected. There are several plastic-strain equi-amplitude with fatigue

life relationships currently available in the literature (e.g., [1] [5] [6] [9] [12], among others) which can be used to estimate the total number of cycles to rupture, N_f, for a given plastic strain, ε_p. Unfortunately, most of the relationships have been calibrated with tests in which buckling was always present thus reducing the fatigue life of the rebars when compared with a buckling restrained specimen tested at the same strain amplitude. For instance, [12] proposed the following empirical equation applicable to all reinforcing steels.

$$\varepsilon_p = 0.08 \cdot \left(2 \cdot N_f\right)^{-0.5} \quad (1)$$

2.2. Energy dissipation and stiffness deterioration

Based on available information such as original calculations, drawings (see Figure 1*a*) and intrusive and non-intrusive investigations, moment-curvature relationships (Figure 1*b*) can be computed for those sections or members showing inelastic deformation. Before assessing a damaged building, however, these relationships should be modified to account for stiffness deterioration and curvature ductility demand (factor conceptually expressed as f_k in Figure 1*d*), as well as for the reduced ability of the reinforced concrete element to dissipate energy after it has been cyclically degraded (factor conceptually expressed as f_E, not schematically shown in the figures). Figure 1*c* shows what the original (baseline) capacity curve would look like when compared with the damaged one, with or without strain-ageing. The loss of the initial (elastic) stiffness will be addressed in a subsequent paper. Regarding the energy dissipation characteristics, [20] provide guidance to estimate the energy dissipation for unrepaired structures. However, damaged specimens, when properly repaired, are still able to dissipate a significant amount of energy, which compares very well with the "as when new" energy dissipation characteristics [2]. Therefore, for repaired structures it is assumed that any loss in their energy dissipation characteristics is insignificant (i.e., f_E equal to 1.0).

2.3. Strain ageing

As explained by [9], some carbon steels display, after it has been submitted to plastic strain, a time and temperature dependent strain ageing effect, which modifies the steel material properties. Research suggests that small additions of Titanium or Vanadium minimise the strain ageing effects. Figure 1*e* shows a stress-strain profile of a rebar made of steel not affected by ageing (black curve) such as steel manufactured with the addition of vanadium [8]. In this case, the bar was strained to a certain level and then unloaded, leading to residual strains. If the bar is aged and loaded again, it will approximately follow the same unaged stress-strain curve. If, however, the steel material is strain-ageing sensitive such as the NZ Grade 300 steel (red curve), when the bar is unloaded, aged and loaded again, there is an increase in the yield and ultimate stresses. In addition, it has been experimentally demonstrated that strain-ageing reduces the ductility (i.e., the strain at rupture) of the bars. The reduction seems to be proportional to the pre-strain level reached prior to ageing (factor conceptually expressed as f_a in Figure 1*f*). Regarding the yield and ultimate stresses, they seem to increase with the increase of the pre-strain level (factors conceptually expressed as $ff_{y,a}$ in Figure 1*g* and $ff_{u,a}$). This increase is more pronounced for the yield stress. Table 1 reports the changes in the lower yield and ultimate strengths due to strain-ageing obtained with NZ Grade 300 steel samples, after being pre-loaded to a certain strain, ε_{peak} [9]. Based on these results, the following factors to account for the increase in the yield and ultimate tensile strengths can be obtained. This increase is important because it can modify the hierarchy of failure thus invalidating the capacity design philosophy.

$ff_{y,a} = 1.16$ (with a standard deviation of 0.07) (2)

$ff_{u,a} = 1.08$ (with a standard deviation of 0.05) (3)

Table 2 reports the following strains at the ultimate tensile strength for aged samples obtained with NZ Grade 300 steel after being pre-loaded to a certain strain, ε_{peak} [9]. Based on these values the following equation can be obtained.

$$\varepsilon_{u,aged} = 19.821 \cdot \varepsilon_{peak}^2 - 3.2507 \cdot \varepsilon_{peak} + 0.2017 \quad (4)$$

Table 1 – Change in the lower yield and ultimate tensile strengths due to strain ageing for NZ Grade 300 steel [9].

Pre-strain, ε_{peak} (mm/mm)	**Lower yield strength (MPa)**			**Ultimate tensile strength (MPa)**		
	Unaged	**Aged**	**Difference**	**Unaged**	**Aged**	**Difference**
0.015	307	388	81	492	499	7
0.030	379	453	74	497	531	34
0.060	432	476	44	489	518	29
0.120	475	527	52	489	546	57
0.180	500	574	74	503	574	71

Table 2 – Summary of the mechanical properties of pre-strained and aged Grade 300 steel samples [9].

Pre-strain, ε_{peak} (mm/mm)	**Vickers hardness (HV_{30})**		**Lower yield strength (MPa)**		**Tensile strength, *UTS* (MPa)**		**Strain at *UTS* $\varepsilon_{u,aged}$ (mm/mm)**	
	Average	**S.D.**	**Average**	**S.D.**	**Average**	**S.D.**	**Average**	**S.D.**
0	150	3.0	322	8.4	507	10.5	0.203	0.002
0.02	168	4.90	388	11.3	501	5.7	0.142	0.020
0.04	180	2.5	436	3.2	521	3.2	0.103	0.005
0.06	191	4.9	490	2.0	533	1.7	0.081	0.002
0.08	198	3.9	512	3.3	536	3.3	0.067	0.002

In equation (4) the coefficients of determination, R^2, is 0.9983, therefore, the model fits the data reasonably well. Since the ultimate strain ε_{UTS} of NZ Grade 300 steel is typically 0.200 mm/mm, then the following factor to account for the reduction of the strain at the ultimate tensile strength can be obtained.

$$f_a = 99.1 \cdot \varepsilon_{peak}^2 - 16.25 \cdot \varepsilon_{peak} + 1.0 \quad (5)$$

2.4. Cyclic deterioration effect of steel strain-life

It can be demonstrated that if a reinforcing bar is cyclically strained during n cycles at ε_{cyclic} for $n < N_f$ cycles, unloaded and then tested monotonically, it will fracture at a strain ε'_{UTS}, where $\varepsilon_{cyclic} \leq \varepsilon'_{UTS} < \varepsilon_{UTS}$. It is believed that this effect is caused by the crack growth phenomena [3]. Thus, the ε'_{UTS} can be estimated as the ε_{UTS} multiplied by the factor f_c conceptually expressed in Figure 1*h*. Although no test results are available for cases where buckling is prevented, it appears that steel subjected to n/N_f equal to or less than 10%, the reduction in the ε'_{UTS} due to the cyclic effect is insignificant [3]. Empirical equations that account for n/N_f greater than 10%, as well as for potential buckling of the rebar will be proposed in a subsequent paper.

2.5. Bond deterioration effect

When a reinforced concrete element is cyclically loaded, the bond between steel and concrete deteriorates. As it deteriorates, the length over which the strains spread out increases, thus reducing the strain for the same curvature ductility demand (factor conceptually expressed as f_b in Figure 1*i*). This factor is implicitly accounted when the relationships between maximum crack widths and peak steel strain were derived (see Section 3).

3. Seismic residual capacity of a plastic hinge

The proposed procedure to account for the seismic residual capacity of a plastic hinge is explained by a worked example. Reference is made to previous concepts described above, as well as to equations developed though Finite Element (FE) modelling. As previously stated, although the procedure can be extended to a more general situation, it has been specifically developed for buildings designed following capacity design principles, where well-detailed beams fail in flexure with a stable hysteretic behaviour.

3.1. Beam section analysis

The first step of the process is to gather all available information such as original calculations, drawings, and intrusive (e.g., concrete and steel material properties, "as-built" dimensions of the structural components, verification of reinforcement content) and non-intrusive investigations (e.g., residual drifts, damage to non-structural components, crack widths and their location, orientation, amount and distribution). For those beams showing inelastic deformation and/or are part of the lateral force resisting system, moment-curvature (i.e., capacity curve) relationships are computed. The capacity curves can be combined with design limits states as required.

Figure 2*a* shows beam cross section with indications of amount and location of reinforcement, as well as the steel and concrete material properties. Section analysis was performed and the moment-curvature shown in Figure 2*b* was obtained. The MATLAB code Cumbia [14] was used for such purpose.

Section analysis provides relationships between beam curvature with applied moment and steel and concrete strains, which are key parameters for assessing the residual capacity of plastic hinges. For this case (i.e., a beam reinforced with NZ Grade 300E steel), it is assumed that the strain at ultimate tensile stress, ε_{UTS}, is equal to 0.20 mm/mm, or 20%.

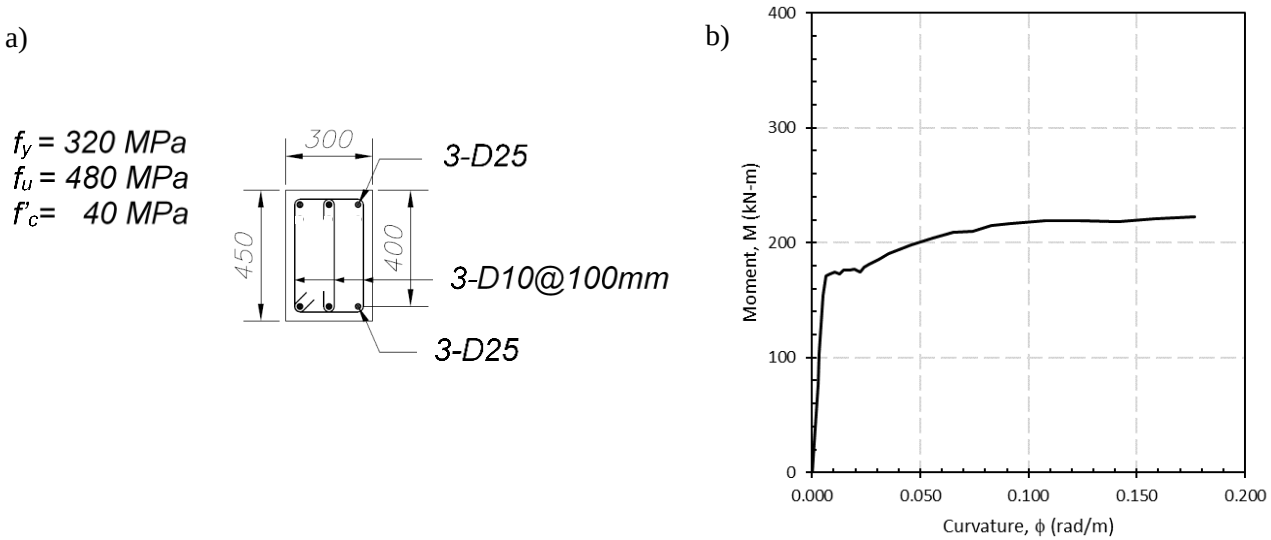

Figure 2 – a) Material properties and beam section details (longitudinal reinforcement ratio ρ_s of 1.23%) used for the section analysis; b) Moment-curvature relationship.

3.2. Mean strain estimation between consecutive flexural cracks

A tentative formulation to relate the mean strain and the peak strain between two consecutive flexural cracks is proposed. The formulation is based on a numerical parametric study using the nonlinear FE code MASA, developed at the Institute for Construction Materials (IWB) of the University of Stuttgart [17]. The formulation is currently being calibrated with additional numerical and experimental investigations.

3.2.1 FE model

Prior to the parametric study the FE model was first validated with the experimental results of a one-half scale reinforced concrete cantilever beam tested at the University of Canterbury [10][11]. The beam is 250 mm wide and 350 mm deep, with a length of 1570 mm measured from the point of maximum moment to the point of load application, assumed to be the beam mid-span or point of contra-flexure in a seismic dominated frame. The beam is reinforced with 4-D16 top and bottom, and stirrups D10 spaced at 75 mm centres over a length of 400 mm, and 125 mm centres in the remaining length of the beam. The steel reinforcement is Grade 300 (f_y 300 MPa). The concrete compressive strength f'_c is 33 MPa. The specimen was subjected to a

quasi-static displacement-controlled monotonic loading until reaching failure. More details on the specimen, instrumentation and testing procedure can be found in [10][11].

Figure 3 shows the monotonic lateral force-displacement response from the quasi-static test. In the same figure, the monotonic curve obtained from the numerical analysis is shown. There is good agreement between this curve and the monotonic response of the experiment for beam rotations. Figure 3 also shows the moment-curvature relationship obtained numerically. Both curves, the force-displacement and moment-curvature, have indications of different limit states. For normal structures, the Serviceability Limit State, *SLS* (Level 1) refers to a 50% probability of exceedance in 50 years intensity level; and the Damage-control Limit State, *DC* (level 2) to a 10% probability of exceedance in 50 years intensity level. The strain limits proposed in [21] were adopted in this study. A parametric study was performed by varying the longitudinal reinforcement content, from 4-D10 (equal to ρ_{min} per [16] to 4-D25 bars top and bottom.

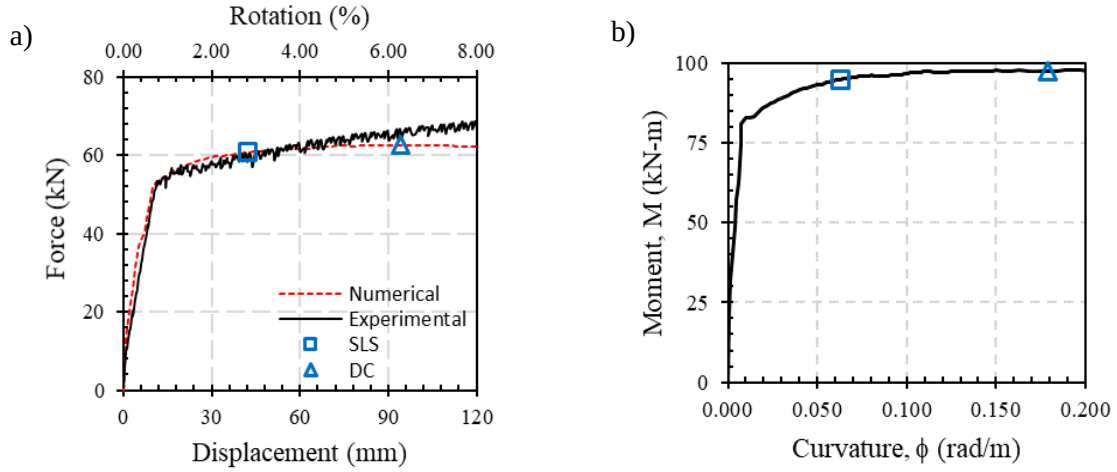

Figure 3 – a) Monotonic lateral response from the experimental and numerical results; and b) moment-curvature relationship obtained numerically. The hollow square represents the Serviceability Limit State (*SLS*); and the hollow triangle the Damage-Control Limit State (*DC*).

3.2.2 Mean strain estimation between consecutive flexural cracks

[21] estimate the maximum crack width as the maximum strain at peak displacement multiplied by the crack spacing. It is believed, however, that it is more appropriate to take into account the strain gradient within the crack spacing, instead of considering its maximum value.

The *fib* Model Code, for strain levels below the yield strain, estimates the mean steel strain over the strain penetration length as 0.60 times the steel strain at the crack. Therefore, using the maximum value as [21] suggest may lead to overestimations of the crack width, in particular at low strain levels. The mean steel strain over a total length of S_{crack}, can be estimated as:

$$\varepsilon_{mean} = \frac{1}{S_{crack}} \cdot \int_{-0.5 \cdot S_{crack}}^{+0.5 \cdot S_{crack}} \varepsilon_s \cdot \delta L \qquad (6)$$

Figure 4 shows the mean steel strain versus the peak strain obtained using the finite element models for zero axial load. As expected, the mean strain depends on the bar diameter and more specifically, on the bond-slip. The bond between two adjacent cracks can be approximated with a parabolic function [18]. The base of the parabola is half of the crack spacing, whilst the height is the maximum (mechanical plus frictional) bond stress that can be developed. Following [7], the maximum bond stress can be defined as follows.

$$\tau_{max} = 20 \cdot f_R^{0.8} \cdot \sqrt{f'_c} \qquad (7)$$

In the previous equation, f_R (unitless) is the related rib area; τ_{max} and f'_c are in MPa.

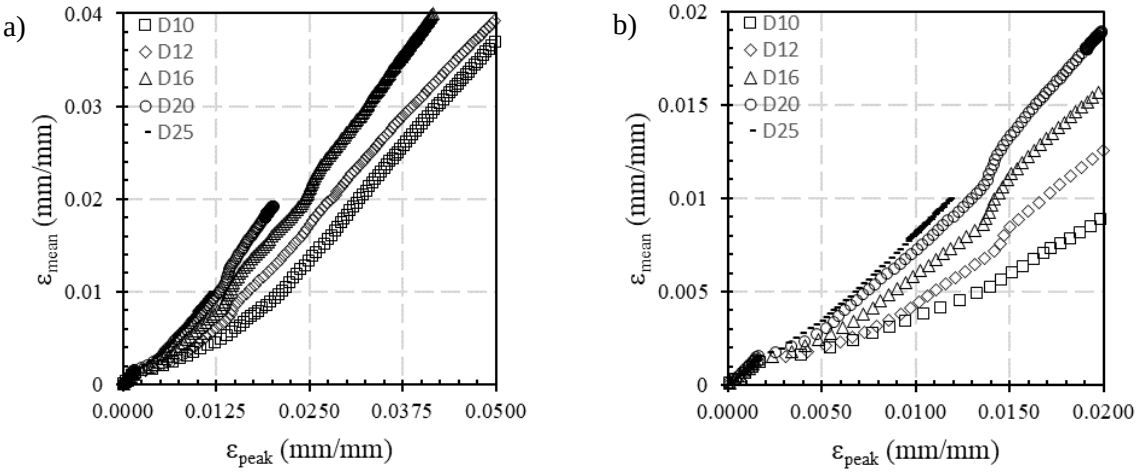

Figure 4 – Mean steel strain over the crack length vs. peak steel strain up to: a) 0.05 mm/mm; and b) 0.02 mm/mm.

Integrating the bond stress over a length equal to the crack spacing multiplied by the crack spacing and the bar perimeter, gives the bond strength developed within the crack spacing. The following equation is obtained by normalizing the bond strength with the bar yield force.

$$\kappa = \frac{53.33 \cdot S_{crack} \cdot f_R^{0.8} \cdot \sqrt{f'_c}}{d_b \cdot f_y} \quad (8)$$

Equation (8) can be considered as a bond efficiency factor. Figure 5*a,b* is obtained by multiplying the mean steel strains of Figure 4 times the bond efficiency factor, κ. It is observed that all the curves except for the most lightly reinforced case (where $\rho_s = \rho_{min}$) follow the same trend. Based on the figure above, for beams with minimum longitudinal reinforcement content as per the [16], the following equations can be used.

$$\kappa \cdot \varepsilon_{mean} = -324.4 \cdot \varepsilon_{peak}^3 + 37.23 \cdot \varepsilon_{peak}^2 + 1.187 \cdot \varepsilon_{peak} \quad \text{(for } \rho_s \geq 0.58\%\text{)} \quad (9)$$

$$\kappa \cdot \varepsilon_{mean} = -219.2 \cdot \varepsilon_{peak}^3 + 32.36 \cdot \varepsilon_{peak}^2 + 1.023 \cdot \varepsilon_{peak} \quad \text{(for } \rho_s = \rho_{min}\text{)} \quad (10)$$

In the previous equations, the coefficient of determination, R^2, is 0.9983 and 0.9979, respectively. It is noteworthy that the following conditions must be satisfied.

$$0.60 \leq \frac{\varepsilon_{mean}}{\varepsilon_{peak}} \leq 1.0 \quad (11)$$

The above equations were developed for beams with no axial load. Figure 5*c,d* shows a comparison of the mean strains in a beam reinforced with D16 bars with no axial load and with $P_u/f'_c \cdot A_g = 0.10$. For the majority of the peak steel strains (up to $\varepsilon_{peak} = 0.025$), the difference between the two curves is negligible. Therefore, the above equations can be used for beams with $P_u/f'_c \cdot A_g \leq 0.10$, which is believed to apply for most situations. It is evident that, in order to estimate the mean strain, the crack spacing, S_{crack}, must be known. [7] proposed the values in Table 3 for the related rib area factor, f_R, based on the bar diameter, d_b.

3.3 Maximum crack widths estimation

Once the mean strain has been estimated, the maximum crack width, w_{max}, can be obtained with the following equation, where S_{crack}= crack spacing; ε_{mean}= mean steel strain over S_{crack}; h= overall depth of the section; kd= neutral axis depth (based on section analysis); h= section depth; and d= effective depth.

$$w_{max} = S_{crack} \cdot \varepsilon_{mean} \cdot \left(\frac{h - kd}{d - kd}\right) \quad (12)$$

Table 3 – Related rib area factors, f_R [7].

Bar diameter, d_b (mm)	Related rib area factor, f_R
10	0.060
12	0.070
16	0.080
20	0.085
25	0.090
32	0.094

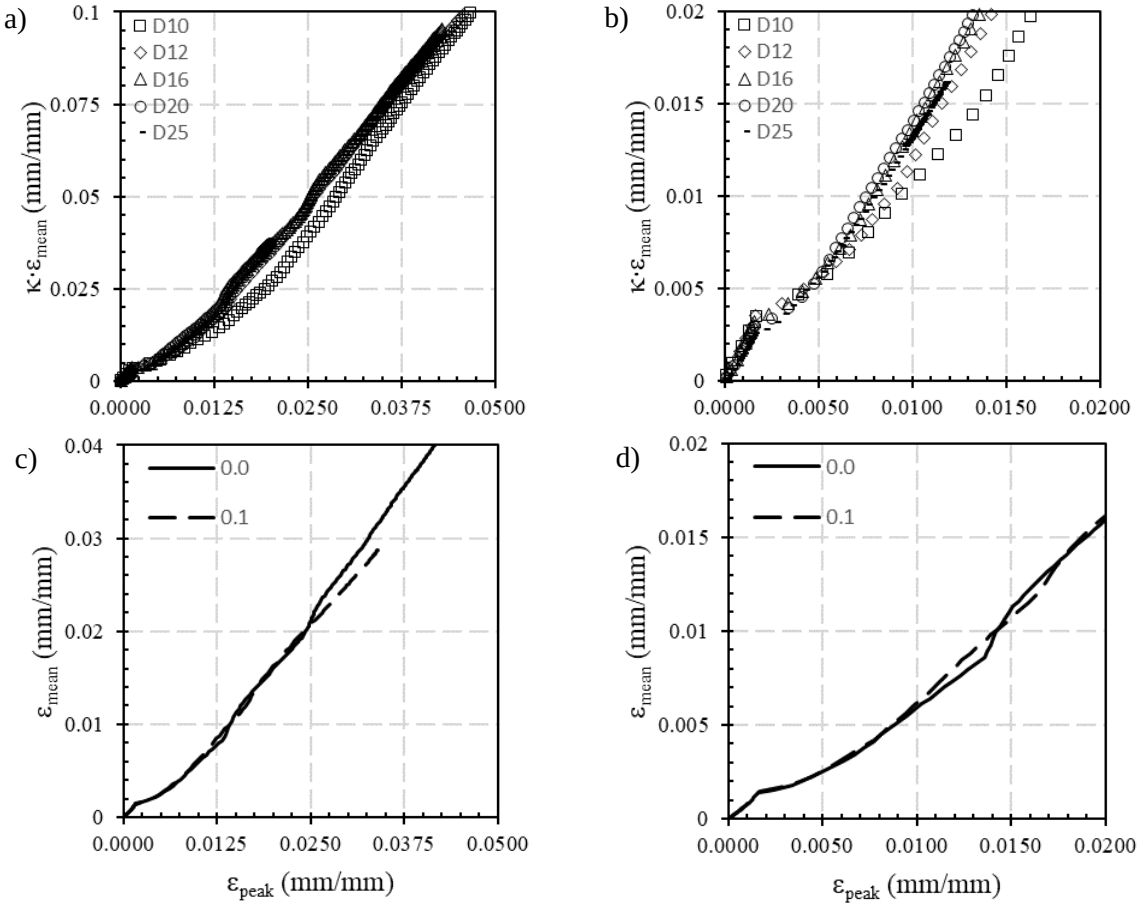

Figure 5 – Mean steel strain, ε_{mean}, times κ vs. peak steel strain $\varepsilon_{peak,}$ for peak steel strains: a) up to 0.05 mm/mm; and b) up to 0.02 mm/mm. Comparison of mean steel strain, ε_{mean}, vs. peak steel strain, ε_{peak}, for peak steel strains: c) up to 0.05 mm/mm; and d) up to 0.02 mm/mm (right), for zero axial force and $P_u/(f'_c \cdot A_g)$ = 0.10, with D16 bars.

3.4 Residual crack widths estimation

As stated in [19] "…*curvature ductility in plastic hinges is achieved primarily by very large inelastic tensile strains. Therefore, the main strain over the depth of a beam and along the length of a plastic hinge will be in tension, resulting in a lengthening of that part of the beam. Because the neutral-axis depth varies along the span, elongations also occur after cracking in elastic parts of the beam. However, these are negligible in comparison with those developed over plastic hinges*." Since the total elongation of the beam can be approximated as the sum of all the cracks formed along the beam (and more precisely within the plastic hinges), we may argue that the ratio of the beam length after load removal upon the beam length at peak displacement (referred as beam length ratio), both measured at the location of the steel in tension, gives an indication of the residual-to-maximum crack width ratio.

Therefore, in Figure 6, the beam length ratios are tentatively assumed as equivalent to crack width ratios (i.e., residual crack width divided by maximum crack width). In Figure 6*a* it is clear how the crack width ratios depend on the beam rotations, and therefore on the beam depth. However, there is no clear relationship between the crack width ratio and the beam rotation. Since the beam rotations depend on the plastic hinge length, which can be related to the beam depth, the same data is plotted against curvature demands as a means to eliminate the dependence on the plastic hinge length. Figure 6*b* shows the results. The scatter in the results is slightly reduced, however there is still a dependence on the beam depth. The crack width ratios are further plotted against the strain in the steel at peak displacement (see Figure 6*c*,*d*). It is evident how all the curves overlap each other. In other words, by eliminating the dependence on the plastic hinge length (from rotations to curvature) and beam depth (from curvature to steel strain), it is possible to develop a unique empirical equation relating the crack width ratios with the strain at peak displacement.

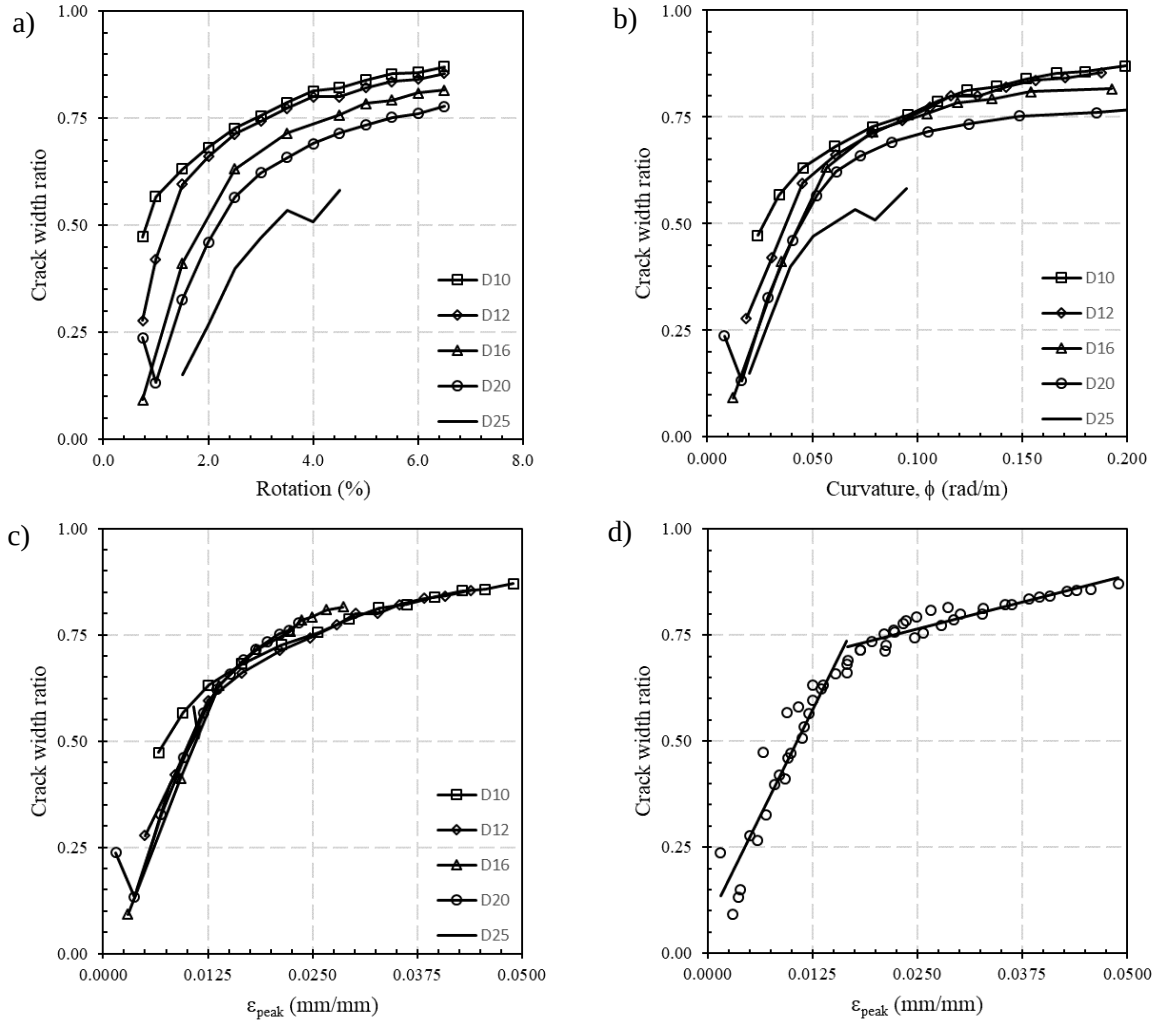

Figure 6 – a) (Res/Max) crack width ratios vs. beam rotation demands; b) (Res/Max) crack width ratios vs. beam curvature demands; c) (Res/Max) crack width ratios vs. steel strains at peak displacement; d) Graphical representation of the empirical relationships between (Res/Max) crack width ratios and steel strain at peak displacement.

The following empirical equations are obtained by linear regression analysis, for beams with $P_u/f'_c \cdot A_g = 0$. The coefficients of determination, R^2, are 0.8843 and 0.8775, respectively:

$$\frac{w_r}{w_m} = 39.9 \cdot \varepsilon_{peak} + 0.075, \quad (for\ \varepsilon_y \le \varepsilon_{peak} \le 10 \cdot \varepsilon_y) \tag{13}$$

$$\frac{w_r}{w_m} = 5.09 \cdot \varepsilon_{peak} + 0.637, \quad (for\ 10 \cdot \varepsilon_y \le \varepsilon_{peak} \le 0.05) \tag{14}$$

Similarly, the following equations were developed for $P_u/f'_c \cdot A_g$= 0.10. The coefficients of determination are 0.9981 and 0.9889, respectively:

$$\frac{w_r}{w_m} = 47.1 \cdot \varepsilon_{peak} - 0.254, \quad (for\ 3 \cdot \varepsilon_y \leq \varepsilon_{peak} \leq 10 \cdot \varepsilon_y) \tag{15}$$

$$\frac{w_r}{w_m} = 12.68 \cdot \varepsilon_{peak} + 0.319, \quad (for\ 10 \cdot \varepsilon_y \leq \varepsilon_{peak} \leq 0.035) \tag{16}$$

3.5 Residual strain capacity and curvature ductility

The residual strain (or remaining strain) capacity, ε_{res}, can be computed as the strain at the ultimate tensile stress, ε_{UTS}, minus the strain at peak displacement, ε_{peak}, plus the strain recovery once the induced load has been removed. It is noteworthy that some assessment guidelines assume the ultimate strain to be much less than the ε_{UTS}. For instance, [13] specifies an ultimate steel strain of 0.05-0.06 mm/mm, or 5-6%. The above can be expressed as follows.

$$\varepsilon_{res} = \varepsilon'_{UTS} - \varepsilon_{peak} + \frac{f_s}{E_s} \tag{17}$$

For cases where there is no strain-ageing (e.g, NZ Grade 500E steel) or cyclic (e.g., preliminary for bars where buckling did not occur and n/N_f is equal to or less than 10%) effects, the strain at ultimate tensile stress, ε'_{UTS} in Equation (17) is equal to ε_{UTS}. The residual strain capacity, *RSC*, is calculated as follows.

$$RSC = \frac{\varepsilon_{res}}{\varepsilon_{UTS}} \tag{18}$$

Another parameter shown in the figure is the peak curvature ductility, μ_ϕ, which can be estimated as the curvature at peak displacement upon the yield curvature.

$$\mu_\varphi = \frac{\varphi_{peak}}{\varphi_y} \tag{19}$$

3.6 Graphic representation of the seismic residual capacity of a plastic hinge

Figure 7*a*,*b* shows a graphic representation of the seismic residual capacity of the plastic hinge of Figure 2 with zero axial load, where strain ageing and the cyclic effect are not of concern. The crack spacing, S_{crack}, was assumed to be 300 mm. In Figure 7*a* the residual crack width, w_{res}, is related with the strain at peak displacement, ε_{peak}, and the residual strain capacity, *RSC*.

On the other hand, Figure 7*b* relates the residual crack width with the residual strain, ε_{res}, and the curvature ductility at peak displacement, μ_ϕ. As an example, a residual crack 4 mm wide measured in this beam, spaced 150 mm crs., corresponds approximately to the strains, curvature ductility and residual strain capacity of Table 4 (see blue arrows in Figure 7*a*,*b*). Judgement is required in order to determine whether the above values are deemed acceptable, or if strengthening/stiffening are required as part of a rehabilitation project. As a reference, [16] states that for well-detailed plastic hinges where the concrete is properly confined by stirrups, curvature ductility values of at least 20 can be achieved during a design earthquake level.

Regarding the residual strain capacity, [4] consider that a strain hardening value (defined as the strain at peak displacement upon the strain at the ultimate tensile stress of the bar) of 15% (i.e., a residual strain capacity equal to or greater than approximately 85%) in flexural dominated walls as a threshold to determine whether strengthening/stiffening is required in addition to epoxy injection of the crack. Strain hardening of 30% or greater requires demolish and rebuild.

Table 4 – Residual strain capacity for a residual crack 4 mm wide.

Parameter	Value
ε_{peak} (mm/mm)	0.03
ε_{res} (mm/mm)	0.17
μ_ϕ (-)	14.5
RSC (%)	85.0

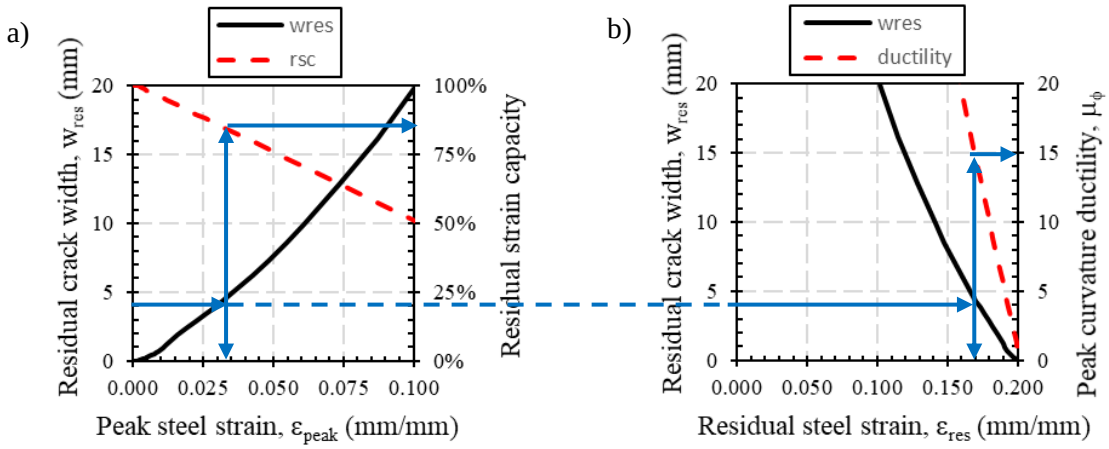

Figure 7 – a) and b) Graphic representation of the residual strain capacity of a plastic hinge.

4. Conclusions and additional comments on the residual capacity of plastic hinges

This paper provides a description of the various factors affecting the residual fatigue life at a component level. It also presents a tentative formulation based on a numerical finite element investigation that relates the maximum and residual crack widths, and steel strain at peak displacement once the onset of nonlinearity has been exceeded. Preliminary equations to quantify the various factors are proposed. Experimental and numerical investigations are currently being conducted in order to validate and calibrate the procedure.

Other factors to consider when assessing the residual capacity of a plastic hinge include:

1. When assessing the seismic residual capacity of plastic hinges, it is important to consider that the effect of strain hardening is very localized. Similar to the capacity design analogy of a chain with one of its links being weaker and more ductile than the others [18], the strains developed during a subsequent load excursion within the bar segment that reached lower levels of strain (i.e., the ductile link in the chain) may be larger than the strains developed within the bar segment that strain hardened (i.e., the brittle but stronger link in the chain). In other words, the bar can self-protect from experiencing a tensile failure. Not surprisingly, [6] observed that the specimens experienced other types of failure prior to a low-cycle fatigue failure. Therefore, strain demands must be considered not only at the point where strain hardening is expected have occurred, but also at adjacent locations.

2. The dynamic effect on the residual crack widths has not been accounted for in the proposed procedure. The residual crack widths from a real earthquake can be much smaller than those predicted with the proposed equations, therefore it can provide unconservative estimates of the residual strain capacity of the damaged bar section. However, the equations developed for the residual crack width estimation are based on the steel strain at the first peak. It was observed that due bond deterioration the peak strain decrease as the number of cycles increase. Therefore, assuming a constant strain equal to the strain measured in the first cycle is a conservative measure.

6. References

[1] Brown, J., Kunnath, S.K. (2004) "Low-cycle fatigue failure of reinforcing steel bars," *ACI Materials Journal*, Vol. 101(6): 457-466.

[2] Cuevas, A., Pampanin, S. (2016) "Post-seismic capacity of damaged and repaired reinforced concrete plastic hinges extracted from real buildings," *16th World Conference on Earthquake Engineering*, Santiago, Chile.

[3] Dowling, N.E. (1977) "Crack growth during low-cycle fatigue of smooth axial specimens," Cyclic Stress-Strain and Plastic Deformation Aspects of Fatigue Crack Growth, ASTM STP 637, *American Society for Testing and Materials*, pp. 97-121.

[4] Engineering Advisory Group, EAG (2013) *Guidance on detailed engineering evaluation of earthquake affected non-residential buildings, Part 3 – Technical guidance, Section 9 – Reinforced concrete buildings*, Revision 6.

[5] Hawileh, R., Rahman, A., Tabatabai, H. (2010) "Evaluation of the low-cycle fatigue life in ASTM A706 and A615 grade 60 steel reinforcing bars," *Journal of Materials in Civil Engineering*, Vol. 22: 65-76.

[6] Kunnath, S.K., El-Bahy, A., Taylor, A.W., Stone, W.C. (1997) *Cumulative seismic damage of reinforced concrete bridge piers*, National Institute of Standards and Technology, NISTIR 6075.

[7] Lettow, S. (2006) *Ein Verbundelement für nichtlineare Finite Elemente Analysen – Anwendung auf Übergreifungsstöße (A bond element for nonlinear finite element analysis – Applied on splices)*, PhD Dissertation, IWB, Universität Stuttgart, Germany (in German).

[8] Loporcaro, G., Pampanin, S., Kral, M.V. (2016) "Effect of strain-rate and material characteristics on the seismic residual capacity of reinforced concrete plastic hinges: numerical investigation," *2016 New Zealand Society of Earthquake Engineering Conference*, Christchurch, New Zealand.

[9] Loporcaro, G. (2017) *A least invasive method to estimate the residual strain capacity of steel reinforcement in earthquake-damaged buildings*, Doctoral thesis, University of Canterbury, Christchurch, New Zealand.

[10] Malek, A., Scott, A., Pampanin, S., MacRae, G.A., Hoult, N.A. (2016) "Damage assessment of RC beam using distributed fibre optics strain sensors," *2016 New Zealand Society of Earthquake Engineering Conference*, Christchurch, New Zealand.

[11] Malek, A. (2018) *Post-earthquake damage assessment and residual capacity of concrete and RC beams*, Doctoral Thesis, , University of Canterbury, Christchurch, New Zealand.

[12] Mander, J.B., Panthaki, F.D., Kasalanati, A. (1994) "Low-cycle fatigue behaviour of reinforcing steel," *Journal of Materials in Civil Engineering*, Vol. 6(4): 453-468.

[13] MBIE, Earthquake Commission, NZSEE, SESOC, NZGS, *The Seismic Assessment of Existing Buildings – Technical Guidelines for Engineering Assessments*, Version 1 – Initial Release, July 2017.

[14] Montejo, L.A., Kowalsky, M.J. (2007) *CUMBIA, set of codes for the analysis of reinforced concrete members*, North Carolina State University, Technical Report No. IS-07-01.

[15] Mukai, T., Kabeyasawa, T., Tani, M., Suwada, H., Fukuyama, H. (2017) "Residual seismic capacity of ductile rc frame with wing walls based on full-scale loading test," *Bulletin of the New Zealand Society for Earthquake Engineering*, Vol. 50(44): 565-573.

[16] NZS 3101:2006 *Concrete structures standard*, Standards New Zealand, Wellington, New Zealand

[17] Ožbolt J, Yijun L, Kozar I. (2001) "Microplane model for concrete with relaxed kinematic constraint," *International Journal of Solids and Structures*, Vol. 38: 2638-711.

[18] Park, P., Paulay, T. (1975) *Reinforced Concrete Structures*, John Wiley & Sons, New York.

[19] Paulay, T., Priestley, M.N.J. (1992) *Seismic design of reinforced concrete and masonry buildings*, John Wiley & Sons, USA.

[20] Pekcan, G., Mander, J.B., Chen, S.S. (1999) "Fundamental considerations for the design of non-linear viscous dampers," *Earthquake Engineering Structural Dynamics*, Vol. (28): 1405-1425.

[21] Priestley, M.N.J., Calvi, G.M., Kowalsky, M.J. (2007) *Displacement-based seismic design of structures*, IUSS Press, Pavia, Italy.

